Journal of Alloys and Compounds, 197 (1993) 281–289
JALCOM 7304

Some electronic aspects of structural maps

Jeremy K. Burdett
Chemistry Department and James Franck Institute, The University of Chicago, Chicago IL 60637 (USA)

Abstract

Three problems are addressed in this paper, stimulated by results presented by the study of structural maps. These are (i) the electronic factors influencing the distortions from symmetric geometries of d^9 and d^{10} systems, (ii) the system-dependent energetics behind the adoption of the cadmium halide and rutile structures for transition metal systems, and (iii) a general picture which relates the structures of solids with one electron count to those found with one or two electrons more.

1. Introduction

The development of structural sorting maps and the organization of the immense body of information they contain encourages us to search for the nature of the electronic reasons underpinning the adoption of one structure type over another. A global theory does not yet exist which serves this purpose, but there have been many studies of smaller subsets of the structural problem. It surely can only be a matter of time, however, before this growing collection of such studies leads to broader insights into the larger structural picture. In this article we discuss three problems of this type.

2. The relationship between some structural chemistry of d^9 and d^{10} systems

The structural features of d^9 and d^{10} systems in which we are interested have been studied for many years, but become strikingly apparent when they are viewed on the structural map. It should be noted from Fig. 1 that both $HgBr_2$ and $CuBr_2$ fall within the structural field containing the CdI_2 and $CdCl_2$ structures [1]. These are just the two simplest polymorphs of structures arising from completely filling the octahedral holes between alternate pairs of close-packed or eutactic anion layers. Rather arbitrarily on the structural map, the "$HgCl_2$" structures are collected together in a separate field, whereas the structures of $CuCl_2$ and $CuBr_2$ are not. However, the structures of both the d^9 and d^{10} examples are significantly distorted away from the "ideal" cadmium halide structure (Fig. 2). Mercuric chloride and bromide show a shortening of two trans linkages. In the $HgCl_2$ structure this is very pronounced

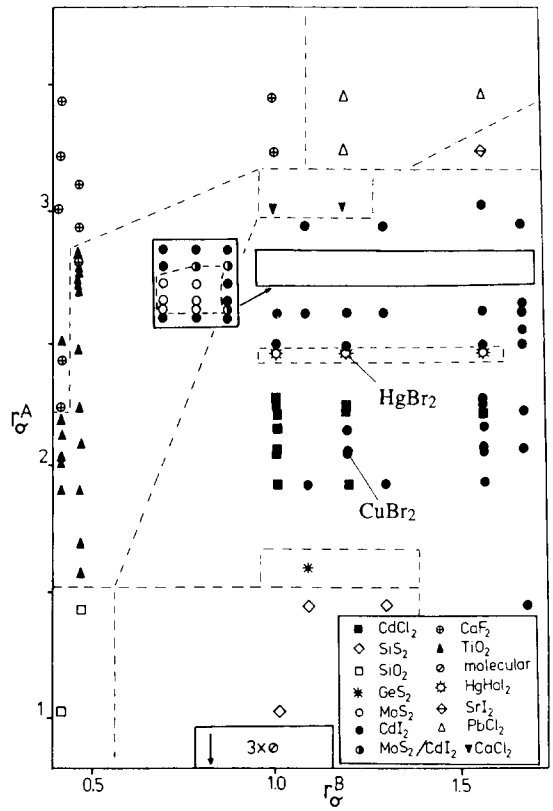

Fig. 1. A structural sorting map (adapted from ref. 1) showing the "$HgCl_2$" structures and those of $CuCl_2$ and $CuBr_2$.

such that the structure consists of linear $HgCl_2$ units packed together such that the structure is far from that of cadmium halide. In the structure of $HgBr_2$ where the distortion is smaller the resemblance to the parent is easy to see. Here the two sets of distances are 2.48 Å(2) and 3.23 Å(4). In the copper halides two trans linkages are lengthened such that the structure

0925-8388/93/$6.00

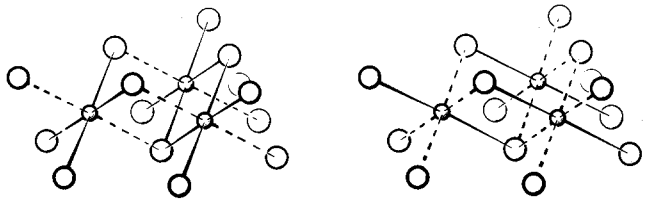

Fig. 2. Distortions of the local octahedral geometry in d^9 (*e.g.* $CuBr_2$) and d^{10} ($HgBr_2$) cadmium halide systems.

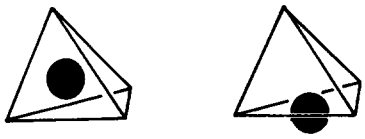

Fig. 3. Distortion of a tetrahedrally coordinated MX_4 unit to the three-coordinate geometry. The picture highlights the possibility of a formally tetrahedrally coordinated ion in a close-packed solid to move from one interstice to another through the triangular "window" in the coordination environment.

is well described as being made up of one-dimensional chains of edge-sharing square planes. The bond lengths are 3.18 Å(2) and 2.40 Å(4). Similar observations are found in AB systems. The structure of cinnabar, HgS, clearly shows the presence of spirals containing linear S–Hg–S units (r(Hg–S) = 2.39 Å(2)) but with four longer Hg–S distances (3.10 Å(2), 3.30 Å(2)) which complete a distorted octahedron around the metal. The structures of AuCl and AuBr show zigzag chains containing linear X–Au–X units.

Tetrahedrally coordinated d^{10} systems are often structurally rather soft, the pathways connecting different coordination geometries being of low energy. The distortion coordinate leading to trigonal planar coordination (Fig. 3) places the metal ion in the face of a tetrahedron of anions, and hence a route in a close-packed material for motion from one interstice to another. Such low energy pathways lead to the occurrence of many ionic conductors [2] with this electronic configuration and specifically with Cu(I) and Ag(I). The softness of the motion associated with this coordination number change is seen to be dramatically apparent in the recent X-ray structure determination [3] of CuP_2VS_6 where the copper is either statically or dynamically disordered amongst three different sites. Quite a variation is seen though, in general, in the size of these distortions. In the structure of metcinnabarite, a higher energy polymorph of HgS, the mercury lies in an undistorted tetrahedral coordination. A large range of distortions is seen for all of the "octahedral" Cu(II) compounds, and a wide variety of structural arrangements for Cu(I) and Ag(I) systems. Such effects lead to the unusual structures of covellite (CuS) and stromeyerite (approximately CuAgS). Traditionally, the structure of the copper d^9 case has been described as the classic case of a first-order Jahn–Teller effect [4], and the mercury d^{10} case as arising via d–s hybridization [5]. We shall show how the details of the picture, via the connections between the two configurations, show a much richer electronic description. These d^9 and d^{10} examples are not the only ones existing as islands within the cadmium halide field. Notice the MoS_2 structure and its stacking variants containing trigonal prismatic metal coordination. These examples are also found only for specific electron counts.

Equation (1) shows the expansion of the electronic energy, $E_0(q)$ for the electronic ground state $|0\rangle$ as a function of some distortion coordinate q in terms of perturbation theory. The idea is to take some (usually high symmetry) structure and test its stability, initially to first order and then to second order if more detail is needed. To this end we give both first- and second-order perturbation corrections to the energy [6, 7].

$$\begin{aligned} E_0(q) &= E_0^0(0) + E_0^1(q) + E_0^2(q) + \ldots \\ &= E_0^0(0) + \langle 0|\partial\mathscr{H}/\partial q|0\rangle q + [\langle 0|\partial^2\mathscr{H}/\partial q^2|0\rangle \\ &\quad - \Sigma_j' |\langle 0|\partial\mathscr{H}/\partial q|j\rangle|^2/(E_j(0) - E_0(0))]q^2 + \ldots \end{aligned} \quad (1)$$

Now let us examine the details of the various terms appearing here. The conditions for a non-zero value of the first-order term, $\langle 0|\partial\mathscr{H}/\partial q|0\rangle$, is that Γ_q, the symmetry species of q, is contained within the symmetric direct product of Γ_0. This leads to the first-order Jahn–Teller theorem, that orbitally degenerate electronic states of high-symmetry molecules will distort so as to remove the degeneracy. The electronic ground state of the d^9 octahedral system is ^2E_g, leading to a distortion coordinate of e_g symmetry via this first-order effect. The d^{10} system is a closed shell and its $^1A_{1g}$ symmetry means that the first-order term is zero here. One pair of distortion coordinates appropriate for the e_g motion is shown in Fig. 4(a). We note that one of them is of the correct form to take an octahedral geometry to the geometry with four short and two long distances and found for virtually all d^9 systems with six identical ligands. Importantly, however, the symmetry description of this first-order Jahn–Teller stabilization gives us no information concerning the details of the distortion and no reason to expect the observation of a distortion of this type. Thus in Fig. 4(b) we show the "Mexican hat" potential [6] as a function of the two coordinates q_1 and q_2 of a. If the distortion coordinate is written in general as $q = q_1 \cos\phi + q_2 \sin\phi$, then for a given $|q|$ the surface is equienergetic for all ϕ. Figure 5 shows the problem on an orbital basis. There is no energetic distinction between the two distortion coordinates shown, namely $\pm q_1$. The only difference is the identity of the upper and lower orbitals. One way often suggested as leading to the observed

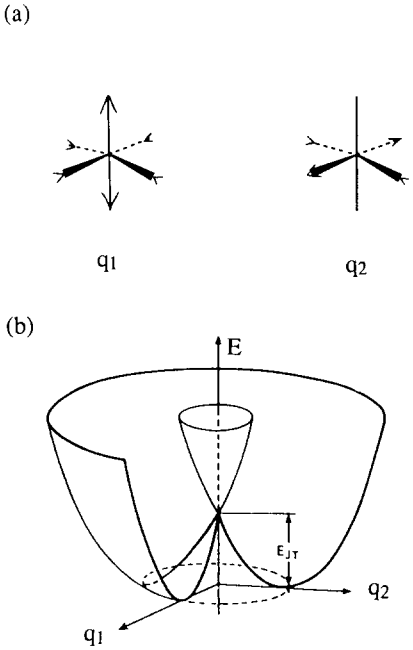

Fig. 4. Distortions of the octahedron. (a) One choice for the two displacement vectors, q_1, q_2. (b) The "Mexican hat" potential function arising via consideration of the first-order term alone in the Jahn–Teller expansion.

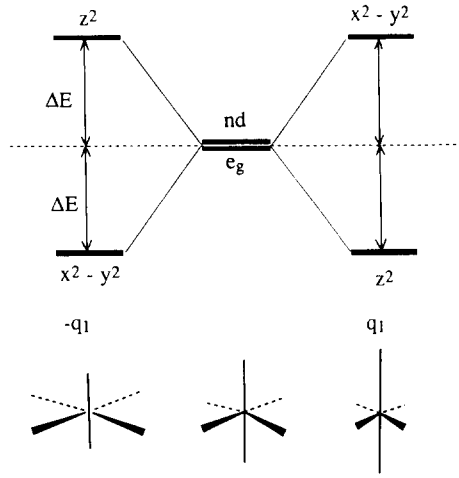

Fig. 5. Behavior of the molecular orbital (largely d) energy levels on distortion of the octahedron, $q = \pm q_1$ using a d orbital only model. Their energetically identical behavior should be noted.

distortion pattern is to add a judiciously chosen "crystal potential" to that shown in Fig. 4(b) which will lead to minima appearing along $q = -q_1$. In terms of the general vibronic picture of these states, the real solution is to investigate the terms quadratic in the distortion. Use of the second-order Jahn–Teller term gives a much more satisfactory picture [8, 9].

The second-order term consists of two parts. The first, $\langle 0|\partial^2\mathscr{H}/\partial q^2|0\rangle$, represents the classical force constant for motion of the nuclei in the frozen electronic charge distribution of the undistorted, $q=0$, structure. The second term, $-\sum_j'|\langle 0|\partial\mathscr{H}/\partial q|j\rangle|^2/(E_j(0)-E_0(0))$, is always stabilizing and competes with the first term to control the overall sign of $E_0^2(q)$. If there is a close-lying electronic state $|j\rangle$ such that the lead term in this expansion can be important, then the possibility exists that $E_0^2(q)<0$ and the system will distort. The symmetry restriction essential for a non-zero value of the numerator is that $\Gamma_q = \Gamma_0 \otimes \Gamma_j$. The symmetry species of both $|0\rangle$ and $|j\rangle$ are of course controlled by the symmetry of the orbitals occupied in the two states. Now the lowest-lying orbital outside the nd manifold of the transition elements is of course the (n+1)s orbital. In the octahedral geometry it will mix during an e_g distortion with the z^2 orbital; in the D_{4h} geometry this mixing continues as the distortion continues. From Fig. 6 we are now in a position to see why the two long–four short distortion is found for the d^9 system but the two short–four long distortion for the d^{10} system. The size of the second-order mixing is inversely proportional to the energy separation, $(E_j(0)-E_0(0))$ of eqn. (1). Identifying this energy gap with the (n+1)s/z^2 separation, the stabilization of z^2 is expected to be larger in the two short–four long case than in the converse ($|\Delta E_1| < |\Delta E_2|$). When all the d orbitals are occupied as in the d^{10} configuration, then the maximum stabilization is seen for the two short–four long case.

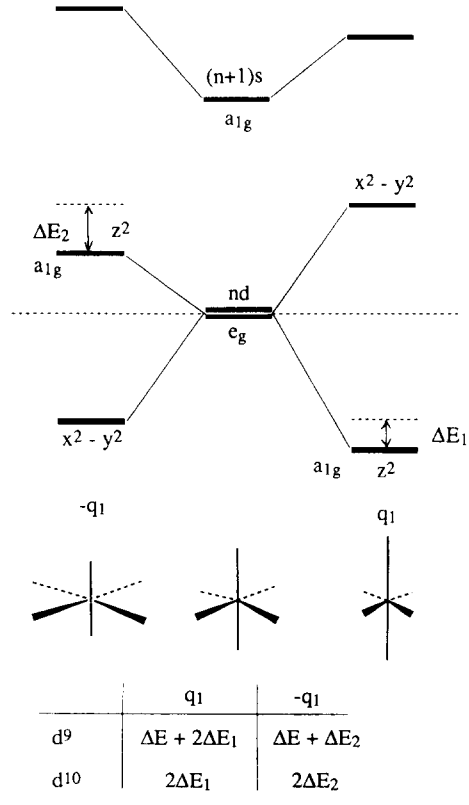

Fig. 6. Effect of d–s mixing on the diagram of Fig. 5. Because of the different energy separations between z^2 and the (n+1)s orbital $|\Delta E_1| < |\Delta E_2|$. The stabilization energy on distortion is shown for the two modes.

For the d^9 configuration the lower energy structure is dominated by the double occupation of the lower energy orbital. The lower orbital is stabilized in the two long–four short case. The inserted table in Fig. 6 shows the energies of the two distortions as a function of d count. A similar discussion applies to the tetrahedral case [10] and is shown in Fig. 7. Here it is the three short–one long distortion which is appropriate for the d^{10} tetrahedron. Such a distortion is just that of Fig. 3 leading to movement of the metal atom to the center of a face of the tetrahedron and the one observed frequently. The approach predicts that it should be the converse, three long and one short, which is appropriate for the "Jahn–Teller" unstable d^9 tetrahedron. In fact the "Jahn–Teller" distortions of tetrahedrally coordinated ions with a degeneracy involving the antibonding t_2 set of orbitals are not usually very obvious. Frequently the crystallographic determination shows undistorted geometries.

Figure 7 shows the general picture, but a more specific analysis of the energetic behavior of the d orbitals around the tetrahedral geometry as a function of the nature of the metal atom is quite enlightening [10]. Is any d^{10} system susceptible to such distortions, or is there something special about copper? Figure 8 shows some energy differences on distortion for two cases, one using orbital parameters appropriate for copper and one using parameters appropriate for iron. Plotted are the sum of the energies of the two sets of e levels and the energy of the a_1 level from the picture of Fig. 7. Recall that it is the behavior of the a_1 level that we have stressed above. Its behavior is quantitatively

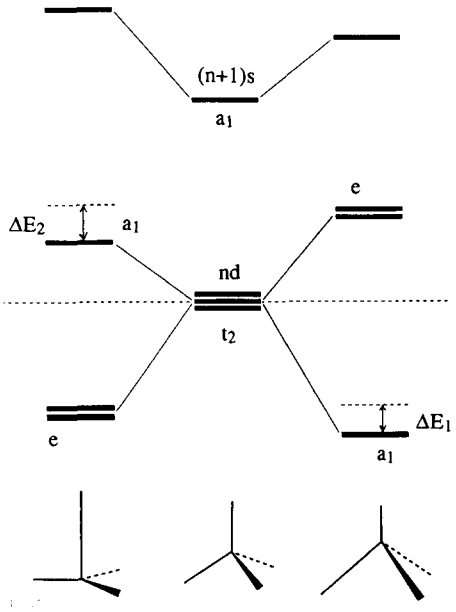

Fig. 7. Effect of d–s mixing in the tetrahedron. Because of the different energy separations between z^2 and the (n+1)s orbital $|\Delta E_1| < |\Delta E_2|$.

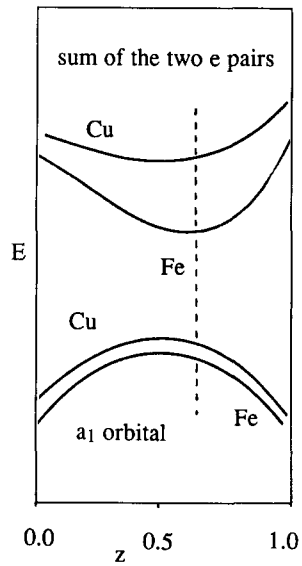

Fig. 8. Energy changes on distortion for the d^{10} configuration. The behavior of the sum of the two sets of e orbitals (one derived from the t_2 set, the other from e of the tetrahedron), and the behavior of the a_1 orbital (derived from the t_2 set). Two plots are shown appropriate for copper and iron parameters. The z parameter measures the displacement of the metal atom from a trigonal plane; the dashed line is the tetrahedral structure.

quite similar in the two cases. The major difference between the two metals lies in the much stiffer potential seen for the e level sum for iron compared with copper. Perturbation theory gives some interesting insights into the differences. The way the perturbation theory is done here is somewhat different from the formalism of eqn. (1). We investigate the energy changes appearing in the different orbital energies on changing the geometry by using this change as the perturbation, $\delta\mathscr{H}$. So for an orbital $|i\rangle$

$$\begin{aligned} E_i(q) &= E_i^0(0) + E_i^1(q) + E_i^2(q) + \ldots \\ &= E_i^0(0) + \langle i|\delta\mathscr{H}|i\rangle \\ &\quad + \Sigma_j' |\langle i|\delta\mathscr{H}|j\rangle|^2/(E_j(0) - E_i(0)) + \ldots \end{aligned} \qquad (2)$$

The first-order correction to the energy of the ith orbital in eqn. (2) is just associated with the effect of changes in the relevant overlap integrals as the geometry changes. Weighted sums over the occupied orbital will give a contribution to the $\langle 0|\partial^2\mathscr{H}/\partial q^2|0\rangle$ term in eqn. (1). The second-order term in this expression clearly has close ties to the second-order Jahn–Teller contribution from eqn. (1). Both first- and second-order energy changes of these orbitals can be calculated numerically for geometries away from the tetrahedral structure. It turns out that the first-order energy changes are always larger for iron than for copper for both a_1 and e orbitals. This is a result of larger iron 3d/ligand overlap compared with the copper case. (On moving to the right of the transition metal series the d orbitals become more

contracted). The second-order energy changes are controlled by s–d mixing for the a_1 orbitals and always stabilize the a_1 (d) orbital, namely z^2. The effect is larger for copper than for iron due to the smaller energy difference between 4s and 3d orbitals on copper. Overall then, the change in the energy of the a_1 orbital is similar for both iron, with the larger first-order change, and copper, with the larger (negative) second-order change. There is, of course, no available empty e set to provide a second-order stabilization of the two pairs of occupied d orbitals of this symmetry (except the 4p orbitals on the metal which are much higher in energy). Taken together they are energetically destabilized as they mix together on distortion. Just as before, this first-order effect is larger for iron than for copper and reflects stronger metal–ligand interactions for iron than for copper. Thus the e symmetry orbitals lead to a larger destabilization on distortion in the iron case.

To summarize then, there is an interesting balance between the first- and second-order energy changes which determines whether the distortion will occur. The 3d orbitals are energetically more important in iron than in copper. This results in the generally larger first-order energy changes for iron with a much more pronounced minimum at the tetrahedral structure associated with the e orbitals for iron than for copper. The second-order Jahn–Teller stabilization is present for both the a_1 orbitals in both systems but is larger for copper. Here the s–d separation is smaller and thus the second-order effect larger from both eqns. (1) and (2). Such a stabilization turns out to be sufficient to win out over the energetic preference of the d orbital manifold alone for the tetrahedral structure in the case of copper but not for iron. In zinc, where the 3d orbitals have disappeared into the core and are therefore not available, the energetic preference of the system is for the tetrahedral structure. In mercury where the relativistic contraction is sufficient to depress the 6s orbital closer to the d orbital manifold, then this second-order term can become important again. The overall electronic picture is quite pleasing.

3. The rutile and cadmium halide structures

The structure maps (Fig. 1) sort many of the double octet AB_2 systems into two structural fields [1], namely that for the rutile (TiO_2) type, found for many oxides and fluorides, and that for the cadmium halide type found for many heavier halides and chalcogenides. (We do not distinguish between the cadmium chloride and cadmium iodide types which differ only in their stacking sequence.) Of interest are the system-dependent factors which determine which is of lower energy. Both structures contain metal atoms in octahedral six-coordination and anions in three-coordination. However, the anions are pyramidal in the cadmium halide structure and planar in the rutile structure. Such an observation encourages generation of a model [11] which identifies the energetic difference between the two structures as being dominated via the difference in anion geometry. Considerable insight into this problem comes from the structures of small molecules. We note that whereas both NH_3 and PH_3 are pyramidal, their inversion barriers differ considerably. That for NH_3 is around 5 kcal mol^{-1}, but that for PH_3 is around 35 kcal mol^{-1}. This means automatically that it is considerably easier to stabilize a planar three-coordinate nitrogen atom in some way than it is to stabilize a planar phosphorus atom. Indeed the $N(SiH_3)_3$ molecule is planar but the $P(SiH_3)_3$ molecule pyramidal. The SiH_3 unit has a low-lying σ^* orbital which may act as a π acceptor with respect to the HOMO of the trigonal planar nitrogen or phosphorus atom (Fig. 9). A similar role is found for this orbital in PR_3 when used as a ligand with transition metals. (Earlier electronic explanations of this effect for Si or P used 3d orbitals in this role but this is not correct.) In rutile a similar stabilizing interaction may occur between metal d and oxygen p. Calculations suggest [12] that this linkage is worth around 10 kcal mol^{-1}.

The origin of the large difference in inversion barrier between first row atoms and their heavier analogs has received much study. In terms of the second-order Jahn–Teller theorem [13] we note from Fig. 10 that the important energy separation between the ground and lowest-lying excited states connects orbitals of a_2'' and a_1' symmetry. Γ_q is thus a_2'' and the correct symmetry to take the planar geometry to the pyramidal one. Since the a_1' orbital is non-bonding, located on the central

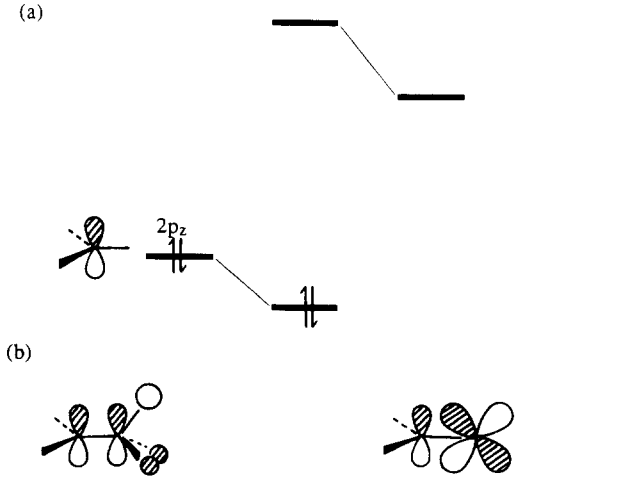

Fig. 9. (a) Stabilization of the planar, three-coordinate atoms by interaction with a π-acceptor. (b) The orbital interaction in the case of nitrogen and titanium atoms.

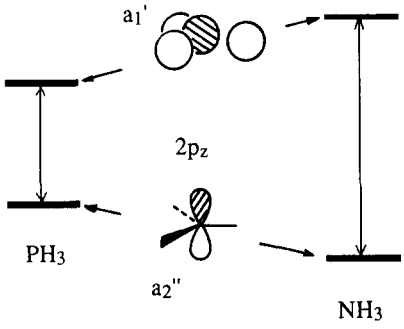

Fig. 10. Second-order Jahn–Teller interaction in eight-electron planar AH_3 molecules. (Note the small gap for PH_3 and the larger gap for NH_3.)

atom, its energy will change in a way dependent on the electronegativity of this atom. It will thus lie deeper in planar NH_3 than in planar PH_3, leading to a smaller energy gap, $(E_j(0) - E_0(0))$ of eqn. (1), for the PH_3 case. In this, the simplest model, the result is a larger driving force for distortion away from the planar structure for PH_3 than for NH_3. Exactly analogous arguments are applicable to the solid state case. A result which will be of interest later is the effect on the geometry of increasing the electron population of the upper orbital. The predicted result is removal or reduction of the driving force for pyramidalization. In fact the first excited state of NH_3 is planar, not pyramidal.

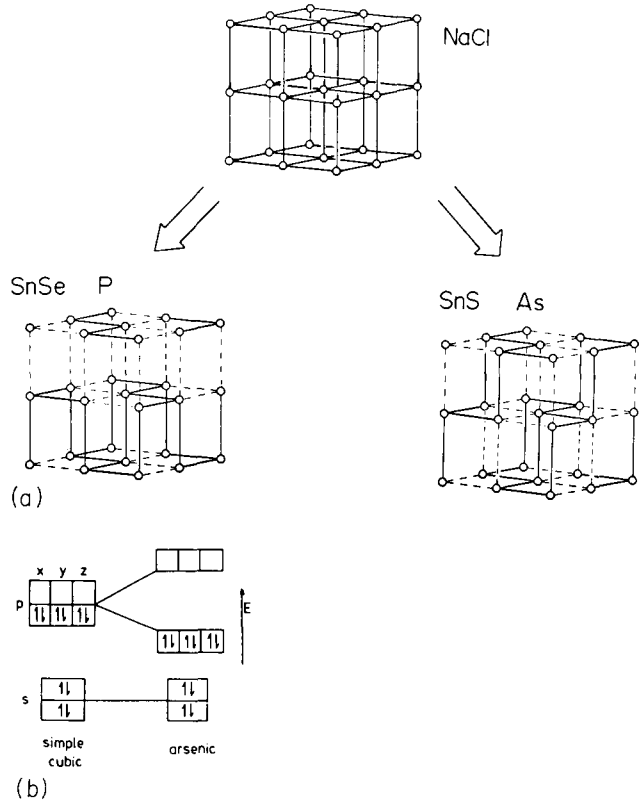

Fig. 11. (a) The three-dimensional Peierls distortion of the simple cubic structure to that of arsenic and black phosphorus. The labels NaCl, SnS, SnSe, indicate some derivative structures. (b) The simplest electronic description which shows half-filled $p_{x,y,z}$ bands for the Group 15 elements.

4. Zeroth, first- and second-order structural changes

It has been long recognized that the variation in electron count leads to some particularly interesting structural changes. Very often the structural changes are quite large so that very different structure maps are used for different e/a ratios. We can use electronic ideas to classify the types of change actually found. As a gross generalization we can envisage the energy levels of molecules and solids as being described as either bonding, non-bonding or antibonding between pairs of atoms in the structure. (We should also recognize that oftentimes a given level may at the same time be bonding between one atom pair but antibonding between another.) Zeroth order structural changes we define as those which take place within the confines of the rigid band model. So, for example, adding electrons to the antibonding part of the d band of the f.c.c. structure of Rh ($a_0 = 3.80$ Å) leads to the larger unit cell appropriate for Pd ($a_0 = 3.89$ Å). First-order structural changes are associated with Fermi surface instabilities, crucially controlled by electron count. One example is the now textbook case of the distortion of the simple cubic structure to that of gray arsenic or black phosphorus when the p bands are exactly half full as they are for the Group 15 elements (Fig. 11). We can envisage such Peierls distortions [14] in a similar way to the first-order Jahn–Teller distortion described above. Second-order changes are then determined by the mixing of higher energy levels into lower energy levels, in a way exactly analogous to the second-order Jahn–Teller approach. For example, the origin of the bond alternation found (Fig. 12(a)) in many perovskites and related structures is the mixing on distortion between the levels at the top of the oxygen p band and those of the metal d band as shown in Fig. 12(b). It should be noted that the gap between oxide and metal levels increases on distortion. In the perovskite example both the top of the lower (full) and the bottom of the upper (empty) orbitals are largely non-bonding in the undistorted structure, but become antibonding and bonding respectively on distortion. Here electron count is important too. The short–long distortions in the perovskite case may be switched off by increasing the electron count so that the upper orbital starts to fill with electrons in exactly the same philosophy employed for the NH_3 molecule described earlier. Figure 12(c) shows [15] that by the time the d^1 configuration is reached then the driving force for distortion has disappeared. ReO_3 is an example of an (empty) perovskite which is cubic.

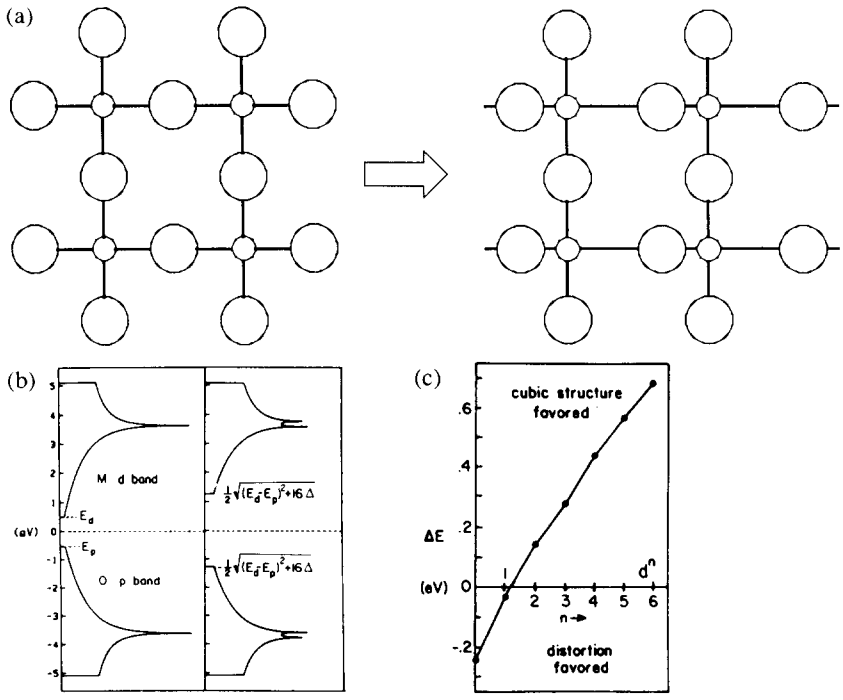

Fig. 12. (a) The distortion of the cubic perovskite structure to one with bond length alternation. Shown is a (100) slice. (b) The second-order mixing of oxygen and metal levels which leads to the distortion, maximized for the d^0 configuration. $\Delta = \beta^2\delta^2$. The two interaction integrals for the short and long distances are $\beta(1+\delta)$ and $\beta(1-\delta)$ respectively. The results come from a calculation [15] with $E_d - E_p = 1.0$ eV, $\beta = 1.8$ eV and $\delta = 0.33$ for the distorted structure ($\delta = 0$ for the undistorted structure of course). (c) Results of tight-binding calculations on the cubic and tetragonally distorted structures with an M–O bond length difference of 0.4 Å.

There is another way to see how a change in the number of electrons leads to geometry changes shown in Fig. 13. Occupation by electrons of the antibonding orbitals of a given structure leads to the generation of repulsive forces between the nuclei. For some systems, such as the transition metal example above, the system may just relax within the same topological framework. In others the driving force for breaking chemical bonds is large. The schematic diagram of Fig. 1 puts the Zintl–Klemm electron counting rules on an orbital basis. Occupation of antibonding orbitals leads to breaking of bonds and generation of lone pair orbitals in such a way as to preserve an octet around each atomic center. Thus (Fig. 14) addition of six electrons to the stable P_4 tetrahedron leads to population of P–P antibonding orbitals, the breaking of three bonds and the generation of six lone pairs in the PCl_3 molecule. The

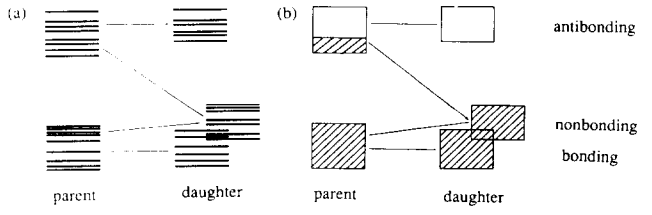

Fig. 13. The changes in energy levels on bond breaking in (a) molecules and (b) solids.

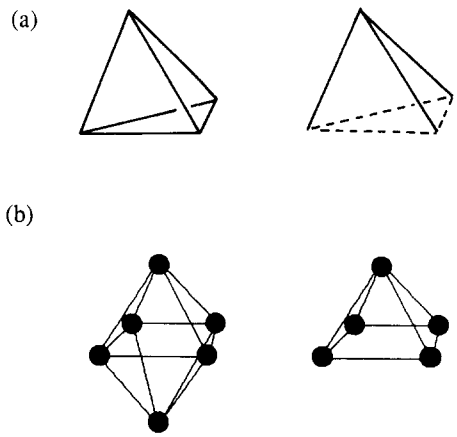

Fig. 14. Structural changes in molecules as a result of added electrons, (a) $P_4 \rightarrow PCl_3$ and (b) $B_6H_6^{2-} \rightarrow B_5H_5^{4-}$ (isoelectronic and isostructural with the known B_5H_9). For clarity the H atoms are not shown.

structural resemblance of the daughter to the parent molecule should be noted. All atoms in both structures have an octet of electrons. A similar geometrical parentage is found in the molecules $B_6H_6^{2-}$ and (the hypothetical) species $B_5H_5^{4-}$. Here, however, the $B_5H_5^{4-}$ molecule (isoelectronic and isostructural with the known B_5H_9), related to the parent by the loss of a BH group, is described accordingly as a nido octa-

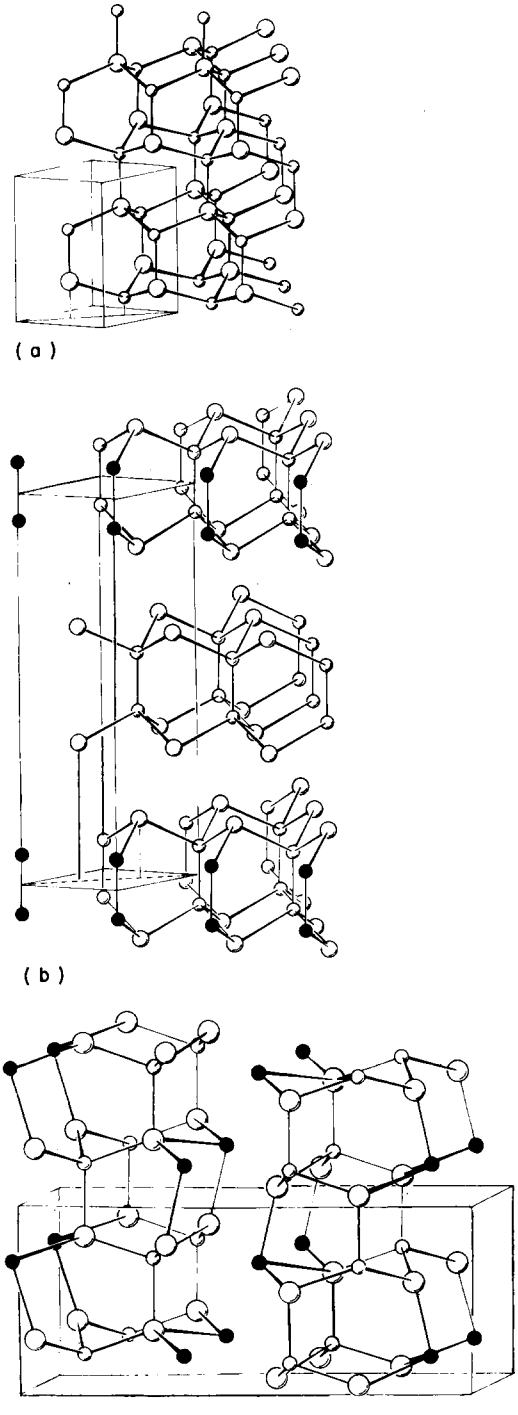

Fig. 15. Structural changes in solids as a result of added electrons, (a) wurtzite → (b) GaSe and (c) wolfsbergite.

hedron. In the daughter molecule, occupied lone pair orbitals point into this vacant site. Both molecules have a total of 14 skeletal electrons as expected from Wade's rules, but a different number of electrons per atom. These two processes show two different ways molecules react to accommodate these extra electrons, ending up in each case with stable electron counts.

We may often view the structures of solids in a related way. Figure 15 shows the structures of β-GaSe (b) and wolfsbergite, $CuSbS_2$ (c), strikingly related to the wurtzite structure (a) by bond breaking. They differ only in the way the bonds between pairs of layers of atoms in the wurtzite structure have been severed: horizontal slices for GaSe and vertical slices for wolfsbergite. Wurtzite is found for many systems with a total of eight electrons per AB unit; both of the other materials have one extra electron. As a result of the bond-breaking process, half of the atoms are now four coordinate and half are three coordinate. (There has in fact been a rearrangement of the atoms in the β-GaSe structure compared with wurtzite, to give Ga–Ga contacts, a change we will discuss below.) The bond-breaking process may be continued, generating the arsenic structure for ten electrons [16].

If wurtzite → GaSe is the solid state analog of Fig. 14(a), is there an analog of 14(b)? The answer is that there is and this process is shown in Fig. 16. Notice that $CdIn_2S_4$ has a defect zincblende structure which may be written as $\square CdIn_2S_4$. Although the electron count per atom in $CdIn_2S_4$ is 4.6 electrons per atom, the number of electrons per site (including the vacancy) is in both structures. This result is well known as the Grimm–Sommerfeld valence rule. The electronic situation for molecules and solids is actually quite similar from Fig. 13. The finite number of atoms and thus chemically important orbitals in molecules are replaced in solids by a finite set of energy bands with properties similar to those of the molecular case. Whereas on bond breaking, individual antibonding orbitals are converted into non-bonding orbitals in molecules, the antibonding band splits off a band of non-bonding orbitals in solids.

In GaSe we noted that the atoms have rearranged compared with the alternating arrangement of the wurtzite parent. This is an observation readily understandable from the electronic picture of Fig. 13. A part of the energetics driving the Gedanken structural breakup is associated with the generation of lone pairs of electrons. The most stable arrangement will then be

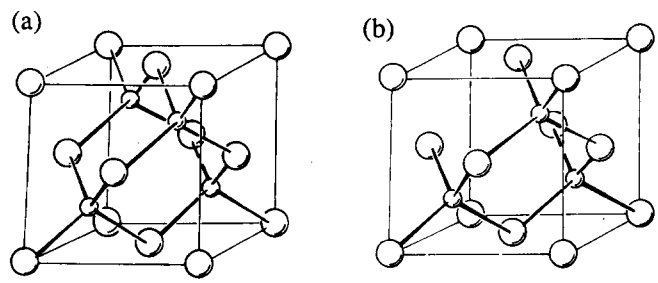

Fig. 16. The generation of the defect structure of $CdIn_2S_4$ (b) from that of zincblende, ZnS (a).

the one where the lone pairs lie on the most electronegative atom, in this case selenium.

Acknowledgments

The ideas of several collaborators appear in this work. It is a pleasure to acknowledge not only O. Eisenstein, T. Hughbanks, S. Lee and S. L. Price, but also L. S. Bartell who introduced me to a broader perspective of the Jahn–Teller theorem.

References

1 J. K. Burdett and S. L. Price, *Phys. Rev. B, 22* (1981) 5462.
2 R. A. Huggins, in A. S. Nowick and J. J. Burton (eds.), *Diffusion in Solids,* Academic Press, New York, 1975, p. 445.
3 E. Durand, G. Ouvrard, M. Evain and R. Brec, *Inorg. Chem., 29* (1990) 4916.
4 For example, F. A. Cotton and G. Wilinson, *Advanced Inorganic Chemistry,* Wiley, New York, 1980, 4th edn.
5 L. E. Orgel, *J. Chem. Soc.,* (1958) 4186.
L. E. Orgel, *Introduction to Transition Metal Chemistry,* Methuen, London, 1966, 2nd edn.
6 I. B. Bersuker and V. Z. Pollinger, *Vibronic Interactions in Molecules and Crystals,* Springer Series in Chemical Physics, Vol. 49, Springer, Berlin, 1989.
7 J. K. Burdett, *Molecular Shapes,* Wiley, New York, 1980.
8 J. K. Burdett, *Inorg. Chem., 20* (1981) 1959.
9 M. Gerloch, *Inorg. Chem., 20* (1981) 638.
10 J. K. Burdett and O. Eisenstein, *Inorg. Chem., 31* (1992) 1758.
11 J. K. Burdett, *Inorg. Chem., 24* (1985) 2244.
12 R. F. Hout, W. J. Pietro and W. J. Hehre, *A Pictorial Approach to Molecular Structure and Reactivity,* Wiley, New York, 1984.
13 L. S. Bartell, *J. Chem. Educ., 45* (1968) 754.
14 J. K. Burdett and S. Lee, *J. Am. Chem. Soc., 105* (1983) 1079.
15 R. A. Wheeler, M.-H. Whangbo, T. Hughbanks, R. Hoffmann, J. K. Burdett and T. A. Albright, *J. Am. Chem. Soc., 108* (1986) 2222.
16 J. K. Burdett, *Nature, 279* (1979) 121.